Pergamon

PII: S0191-8141(97)00042-4

Journal of Structural Geology, Vol. 19, No. 9, pp. 1173 to 1187, 1997

0191-8141/97 $17.00 + 0.00

Shear fracture pattern and microstructural evolution in transpressional fault zones from field and laboratory studies

J. V. A. KELLER*

Fault Dynamics Project, Department of Geology, Royal Holloway, University of London, Egham, Surrey TW20 0EX, U.K.

S. H. HALL

Strucoil, 115 Greenwich South Street, Greenwich, London SE 10, U.K.

and

K. R. McCLAY

Fault Dynamics Project, Department of Geology, Royal Holloway, University of London, Egham, Surrey TW20 0EX, U.K.

(*Received* 20 *November* 1996; *accepted in revised form* 14 *May* 1997)

Abstract—Zones of transpressional shear deformation accommodate strike-slip and oblique-slip displacements. Field work in a transpressive shear zone, and transpressional analogue clay-box modelling, show that a P-oriented foliation and associated P-shears are preferentially developed over the more common R_1 Riedel-shears. The Carboneras fault system (CFS) in SE Spain is a left-lateral transpressional shear zone with an internal geometry characterized by first-order Y-oriented faults and widespread P-oriented second-order faults. The mesoscopic to microscopic gouge fabric reflects the regional architecture of the shear zone being dominated by a pervasive P-oriented foliation and discrete Y- and P-shears. Friction experiments carried out to investigate the textural evolution of gouge fabrics showed four textural stages of fabric development, from foliation formation to extreme shear localization resulting in cross-gouge failure. Transpression clay-box models favoured the formation of secondary P-oriented shear fractures and P-oriented shear lenses. Further deformation caused differential shear lens rotation and shear lens orientations closer to the mean displacement direction. Our field studies and laboratory analogue experiments indicate that shear zones dominated by P-shears are diagnostic of a transpressional deformation regime. © 1997 Elsevier Science Ltd.

INTRODUCTION

The internal structure and fabrics of brittle shear zones has been an important objective of structural and rock mechanics research. A great deal of experimental work has been performed over several decades in order to investigate the fault patterns developed during fault zone evolution. These modelling studies successfully reproduced the secondary fracture patterns developed in natural shear zones (Tchalenko and Ambraseys, 1970; Wilcox *et al.*, 1973; Logan *et al.*, 1979) and establish a sequence for the development of commonly observed secondary shear fractures, starting with R_1 Riedel-shears, P-shears and finally Y-shears. Eventually, as movement continues, most of the fault displacement is accommodated by the Y-shears (Logan *et al.*, 1979). Renewed interest in the study of secondary shear fractures within fault zones has been sparked by results that suggest that their geometry and degree of development is related to the sliding behaviour of the fault zone (Logan *et al.*, 1979; Moore and Byerlee, 1991; Chester *et al.*, 1993). Most of these studies, however, have discussed the internal fabric assuming a standard simple strike-slip regime of deformation and the resulting geometries are explained according to Coulomb–Mohr theory, without taking into account the possibility of oblique-slip displacements.

The widespread occurrence of P-shears in natural wrench fault zones has not been fully addressed in the literature and cannot be explained solely by the Coulomb–Mohr failure criterion. Furthermore, the synchronous development of P- and R_1 Riedel-oriented shears is still a poorly understood phenomenon (cf. Bartlett *et al.*, 1981). Naylor *et al.* (1986) have explained the secondary formation of P-shears in sand-box experiments of strike-slip faulting by the rotation of the stress field in the regions between R_1 Riedel-shears. In addition, Naylor *et al.* (1986) attributed the (almost) simultaneous development of P- and R_1 Riedel-oriented shears reported by Bartlett *et al.* (1981) to be a result of the elastic stiffness of the modelling material (limestone) used in their triaxial experiments. Because of the elastic stiffness of limestone, and the experimental set-up used in Bartlett *et al.*'s models, P-shears formed earlier than expected as the

*Present address: Department of Geology and Geophysics, The University of Calgary, Calgary, Alberta, Canada T2N 1N4.

developing R_1-shears can only accommodate very limited amounts of displacement. In this paper, we attribute both phenomena to deformation within a zone of oblique-convergent (transpressional) displacement. A brittle transpressional shear zone in SE Spain was studied in order to investigate the geometry and the development of the internal gouge fabric. Special attention was given to the common occurrence of P-shears in relation to R_1 Riedel-shears within the shear zone. Direct shear friction experiments were carried out to investigate the progressive evolution of gouge microstructures, whereas physical clay-box modelling was conducted in order to understand the geometric evolution of the secondary shears within the fault zone. In particular, we aimed to investigate whether a fault zone architecture characterized by P-oriented fracture sets is the result of oblique-convergent (transpressional) shear displacement.

REGIONAL SETTING

The Betic Cordillera of SE Spain is an ENE–WSW-trending Alpine orogenic belt of Eocene–Miocene age (Lonergan, 1993). The Betic Cordillera has been divided into a non-metamorphic External Zone in the north and a metamorphic Internal Zone in the south (Fig. 1). The External Zone is primarily composed of Mesozoic–Tertiary continental margin sedimentary rocks, whereas the Internal Zone consists of stacked-up Palaeozoic and Mesozoic metamorphic and sedimentary rocks.

Deformation and metamorphism occurred from the Eocene to Early Miocene (Bakker *et al.*, 1989; Lonergan, 1993) in the Internal Zone with thin-skinned thrusting and folding migrating towards the External Zone in the Miocene (García-Hernández *et al.*, 1980; Banks and Warburton, 1991). Extensional deformation and collapse followed in the Late Oligocene–Miocene (Doblas and Oyarzun, 1989; Platt and Vissers, 1989) culminating with the opening of the Alboran Sea (Fig. 1). Basement highs in the Internal Zone are separated by Neogene basins that have been suggested to have resulted from the Miocene extensional collapse (e.g. the Huercal-Overa basin; Doblas and Oyarzun, 1989; Platt and Vissers, 1989) (Figs 1 & 2). However, some of these basins were formed along major strike-slip faults and their evolution interpreted to be kinematically linked to the strike-slip deformation (e.g. Níjar and Vera basins; Montenat *et al.*, 1987; Sanz de Galdeano, 1990).

The study area is located to the northeast of the town of Almería, along the eastern margin of the Níjar basin and the Sierra Cabrera basement high, where the transpressional Carboneras fault system (hereafter called CFS) cuts across the basin from the northeast to the southwest (Fig. 2). The CFS is extremely well exposed along most of its strike, but exceptional exposures occur along the south and east sides of the Sierra Cabrera basement high, to the west of the town of Carboneras and in the La Serrata ridge (Fig. 2).

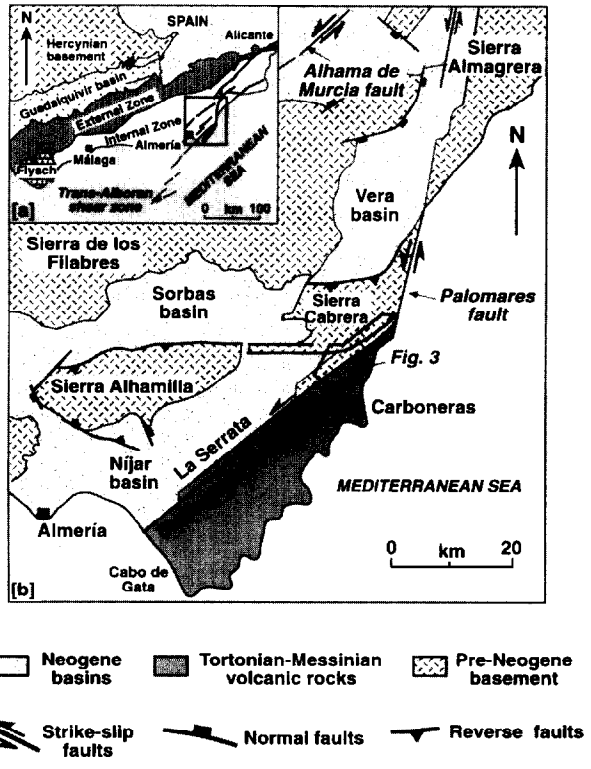

Fig. 1. (a) Simplified regional geological map of southern Spain showing the tectonic provinces of the Betic Cordilera, modified from Weijermars (1991). The location of the studied area as well as the Trans-Alboran shear zone is indicated. (b) Tectonic map of the Almería area in the internal Betic zone, showing the location of the Carboneras fault system and other shear zones discussed in the text, and the distribution of Betic basement blocks and main Neogene basins (modified from Keller *et al.*, 1995). Location of Fig. 3 is marked.

FIELD STUDIES

The Carboneras fault system

In the Almería region, the CFS cuts through the stacked metamorphic units exposed in the basement highs that form the Internal Zone of the Betic chain (Figs 1 & 2). The CFS consists of a long linear network of NE–SW-trending left-lateral strike-slip faults, with individual lengths in the order of tens of kilometres. The northern part of the fault zone is linked to the N–S-trending Palomares fault, forming part of a regional left-lateral shear zone (the Trans-Alboran shear zone; Larouzière *et al.*, 1988), which extends for hundreds of kilometres from Almería in the south to Alicante in the north (Fig. 1).

Miocene–Recent left-lateral oblique-slip (transpressional) was accommodated along the CFS (Hall, 1983; Rutter *et al.*, 1986). A previous joint orientation study (Fournier, 1980) has indicated that the maximum principal stress σ_1 changed from NE–SW to NW–SE at the end of the Early Neogene. As a result, the nature of displacement along the fault system changed from mainly left-lateral strike-slip to left-lateral transpression. The CFS has been active from the Burdigalian to the

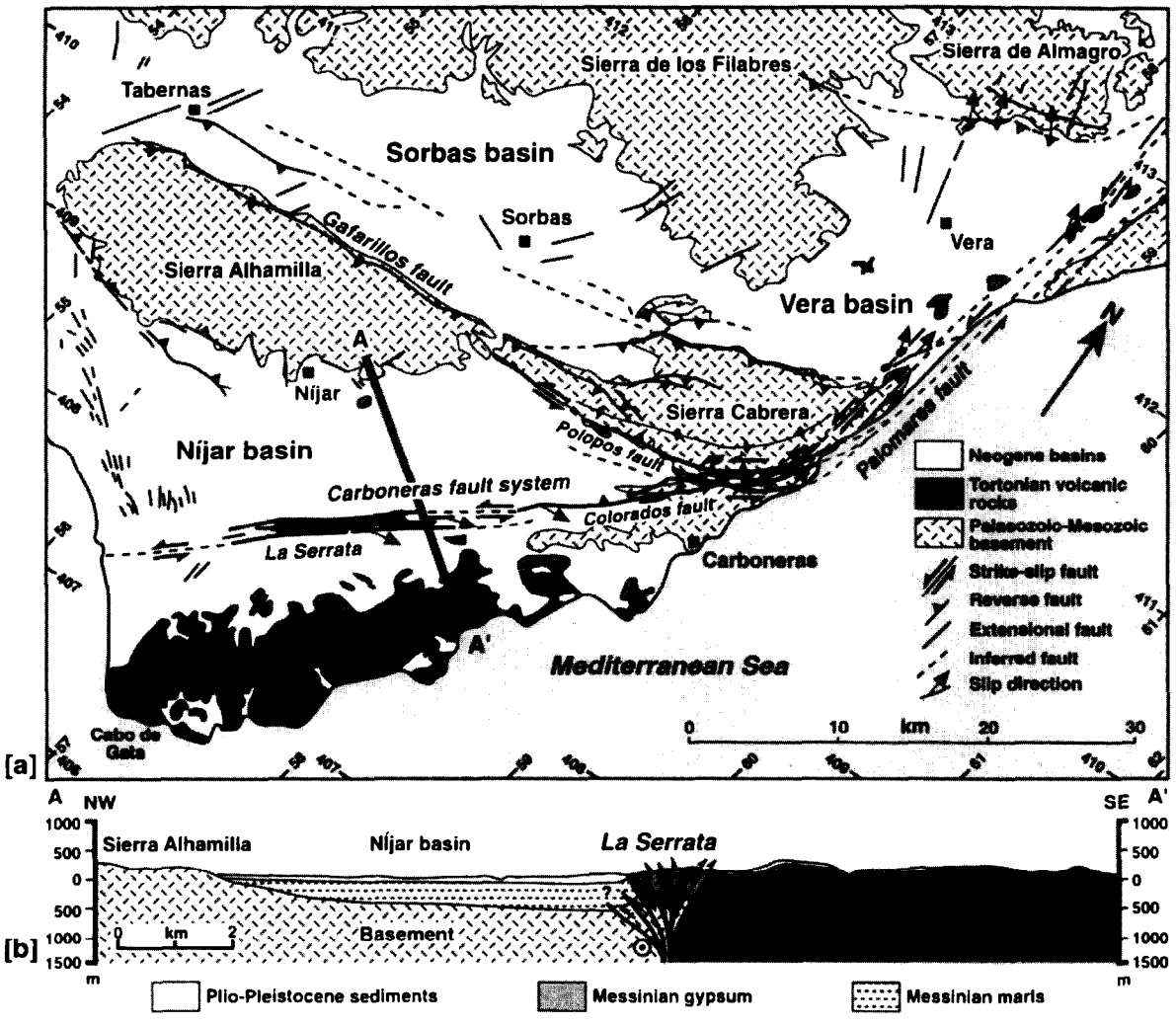

Fig. 2. (a) Tectonic map of the Níjar and Vera basins locating the main Palaeozoic–Mesozoic basement culminations and the main fault zones in the area. Kinematic data from slip lineation measurements in the CFS and Palomares fault is shown. (b) Geological cross-section through the Níjar basin illustrating the internal geometry of the CFS in the La Serrata area, which forms a characteristic positive flower structure.

present, with fault movement being laterally transferred, and accommodated, by different branches of the CFS through time (Keller *et al.*, 1995). A component of reverse-slip, mainly to the southeast but with local variations, is readily observed along the CFS (Fig. 2a & b). Transpressional reverse faults created topographical highs, such as La Serrata, where deeper rocks have been exposed (Fig. 2). Reverse faults also expose basement rocks in the Sierra Cabrera associated with a restraining bend to the north of the town of Carboneras (Figs 1 & 2).

To the south of the Sierra Cabrera block the CFS branches out and forms three separate fault zones; the Polopos, Sopalmo and Colorados faults (Fig. 3) (Hall, 1983; Keller *et al.*, 1995). Individual faults are commonly steeply dipping, usually towards the NNW. The most significant faults, in terms of their thicknesses (m-scale cataclastic zones of deformation) and field relations, were designated as first-order structures. Secondary faults associated with the first-order ones, especially splays to the principal faults, were defined as second-order ones (Fig. 3).

The internal architecture of the CFS is defined by km-scale relatively unstrained fault-bounded blocks (shear lenses) that exhibit a characteristic stratigraphic sequence. Displacement along the CFS has juxtaposed shear lenses of different structural levels, as for example across the northern part of the Colorados fault zone. From the northwest to the southeast the shear lenses consist of: (1) pre-Neogene basement black slates and schists; (2) a series of slates, phyllites and dolomites; (3) red sandstones, dolomites and limestones; and (4) Burdigalian marls and volcanics. Typically, the shear lenses are bounded by first-order Y-oriented slip zones and interlinking E–W to NW–SE second-order faults with oblique reverse offsets and orientations characteristic of P-shears (Keller *et al.*, 1995) (Fig. 3a & b). This linked system of first- and second-order faults forms a complex anastomosing pattern with shear lenses occurring adjacent to or between first-order faults. The

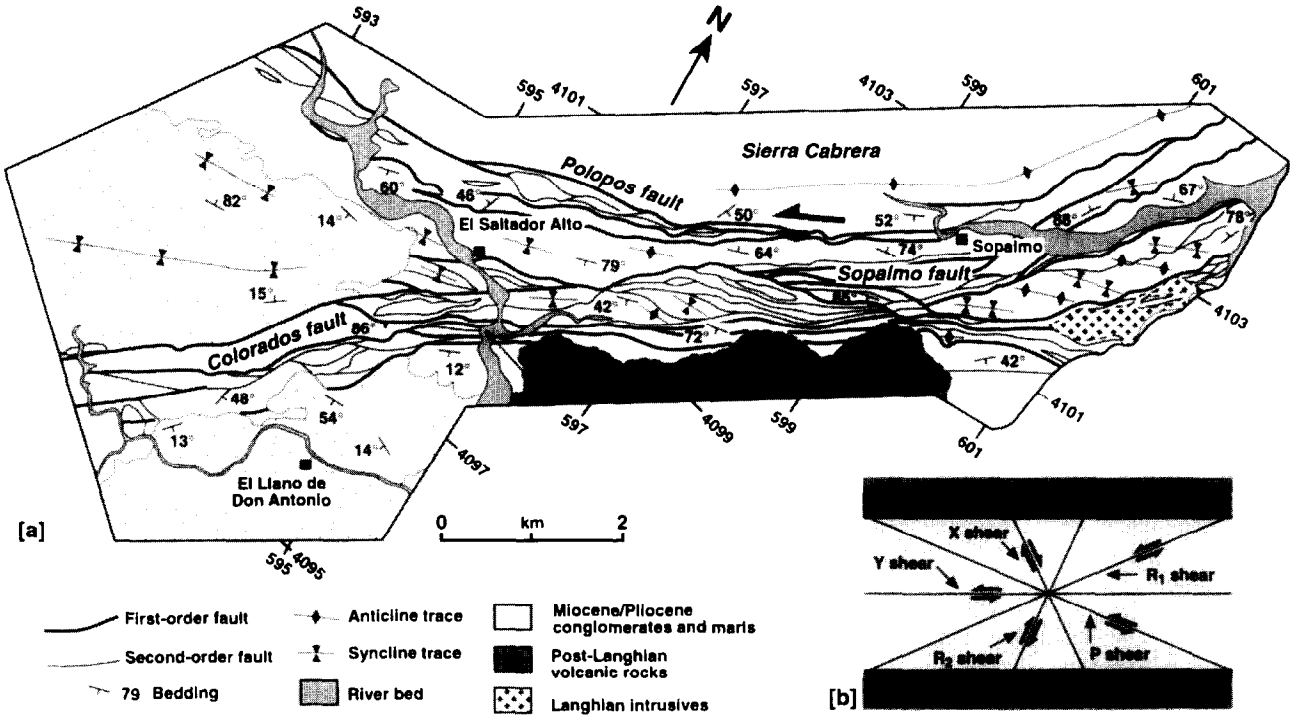

Fig. 3. (a) Detailed structural map of the northern part of the CFS modified from Keller *et al.* (1995) showing the distrubution and orientation of first- and second-order faults as well as associated anticline–syncline pairs (indicative of left-lateral transpressional displacement). Note the characteristic P-orientation of the secondary shear faults. (b) Diagram showing the orientation and sense of movement of shear fractures developed within gouges during deformation according to the labelling convention of Logan *et al.* (1979).

anastomosing geometry of the slip zones is observed across a wide range of scales and the resulting foliation is characteristic of the abrupt strain transitions in shear zones.

Wrench folding associated with left-lateral motion of the CFS is relatively common. Well-exposed meso-scale folds are seen to the east of the locality of Sopalmo (Fig. 3), where ESE–WNW-trending en échelon upright folds occur in a narrow belt (a few hundreds of metres long) parallel to the CFS. En échelon folds are generally oriented at less than 45° (usually between 15° and 30°) to the first-order faults, which is interpreted to be a result of the transpressional deformation. Different episodes of fault movement and wrench fold formation were identified, with some fold sets being cut by second- and/or third-order faults, whilst other sets appear to be related to fault movement along the same faults. Along the restraining bend on the southern side of the Sierra Cabrera basement schists were folded during transpression and form an asymmetric anticline parallel to the CFS (Fig. 2). Parasitic folding developed in the anticline's southern limb with the folded bedding showing meso-scale fold hinges also parallel to the CFS.

P-shears

The second-order faults within the CFS characteristically show E–W to ENE–WSW strikes, which correspond to P-shear orientations (Fig. 3a & b). They form angles between 12° and 27° to the first-order Y-oriented faults, whereas usual values are expected to be in the order of 10–15° (Naylor *et al.*, 1986; Moore *et al.*, 1989). Riedel-oriented second-order faults (NE–SW trending) also occur, and can be as common as the P-oriented ones. Faults exhibiting small displacements (few centimetres), or in the early stages of fault evolution, show synchronous development of P- and Riedel-shears (Keller *et al.*, 1995). P-oriented shears are also commonly observed on a centimetre to microscopic scale within the fault gouge (see next section). This internal architecture defined by the predominance of P-oriented faults is also observed at map scale in the La Serrata area (Fig. 2a) and between the localities of El Saltador Alto and Sopalmo (Fig. 3). In these two localities shear lenses are oriented in the P-direction and bounded by ENE–WSW-trending (P-oriented) second-order faults. In the La Serrata area displacement appears to have been partitioned within a 2–3 km wide zone of deformation bounded by two main parallel faults (Fig. 2a). Locally, steeply dipping P-oriented second-order faults link the two principal faults forming lensoidal blocks or typical shear lenses (Fig. 2a). The two main bounding faults (as well as several second-order faults) display reverse offsets, with the north fault showing NW-vergence and the south fault SE-vergence (Fig. 2a & b). In cross-section the geometry of the CFS in the La Serrata area is that of a flower (tulip) structure, formed within the left-lateral transpressional fault system (Fig. 2b).

P-oriented fault traces can exhibit distinct sigmoidal

geometries in map view (e.g. between El Saltador Alto and Sopalmo; Fig. 3), suggesting that a component of block rotation was accommodated in the CFS. At outcrop scale, left-lateral paired faults are sometimes connected by right-lateral sigmoidal second-order shears, which indicate a counter-clockwise rotation about a vertical axis. Typically, the second-order P-oriented faults link paired first-order structures, nucleating at one fault and merging with the opposite one. Their geometry, together with the identification of seven periods of fault activity, was attributed to incremental finite displacements along the first-order faults and lateral displacement transfer between faults (Keller *et al.*, 1995). The model required P-oriented shears to have formed at the tips or stick-points along the first-order faults as shear strain increased during individual tectonic episodes (Keller *et al.*, 1995). As a result, the second-order P-shears developed to transfer and partition displacement between different first-order fault strands.

Field and experimental studies have shown that Riedel (R_1)-shears are usually the most common shear fabric present in strike-slip shear zones (Tchalenko, 1970; Rutter *et al.*, 1986; Evans, 1988, 1990). R_1 Riedel-shear systems are also known to form the precursor and the controlling structures in the overall geometry of strike-slip zones (Freund, 1974; Hempton and Neher, 1986; Naylor *et al.*, 1986), and form at a critical stress level in response to Coulomb failure (Mandl *et al.*, 1977). However, Coulomb failure does not explain either the predominant development of P-shears, or its synchronous formation with Riedel-shears, in shear zones. As described above, however, the meso- and microscopic fabric in the CFS is characterized by P-oriented shears in contrast to R_1 Riedel-shears. This is attributed to the transpressional regime of deformation. Moreover, Keller *et al.* (1995) have proposed that P-oriented shears are characteristic of oblique-convergent transpressional fault zones, and may be used as diagnostic of this deformation regime in the field. Physical clay-box experiments (see below) were carried out to test this assumption.

GOUGE FABRICS

Outcrop scale

Fault zones within the CFS are typically composed of m-thick layers of fault gouge. Some fault zones can be hundreds of metres thick and exhibit several gouge types. The fault gouge consists of cm- to m-scale bands of a very fine clay-rich matrix with mm- to cm-scale clasts. At the northeast end of the CFS, near the locality of Sopalmo, the *Rambla de Granatilla* valley exposes a superb section of fault gouges across the Colorados fault zone (for location see Fig. 3). In this area, the Colorados fault zone shows a complex arrangement of shear lenses with up to 10 types of fault gouges and microcataclasites, for a thickness of nearly 200 m. The different fault rock types include black (graphite schist) gouge, yellow marl gouge, black schist gouge, red sandstone gouge, carbonaceous gouge, andesite microcataclasite and gouge, purple phyllite gouge, red sandstone and phyllite gouge and microcataclasite, graphitic quartzite cataclasite and red sandstones. This section was investigated in detail and samples of the different fault gouges were collected for thin sections and frictional experiments.

Three main planar features, R_1-, P- and Y-shears, are recognized in the Rambla de Granatilla gouge zone (Fig. 3b) (Logan *et al.*, 1979; Rutter *et al.*, 1986). When exposed, any of these types of secondary shear plane can show a strong linear fabric, which in the Y-shears is parallel to sub-parallel to the fault-slip direction. Surface polishing, associated with mechanical wear grooves (slickensides) and/or crystal fibres, is also widespread. The majority of the slickenfibres indicate left-lateral displacements with few, outcrop-scale, faults exhibiting right-lateral movement (Keller *et al.*, 1995). Striae observed on the northern portion of the CFS, in the Sierra Cabrera basement block, show N–S orientation whereas towards the south, and especially in the La Serrata area, striations show a more NE–SW trend (Fig. 2a).

The most pervasive planar fabric in the gouge is a P-oriented foliation which is commonly associated with P-oriented shears. The P-planes are oriented at between 165° and 170° to the slip direction, in close proximity to the maximum finite flattening plane. However, P-planes inclined at higher angles (135–140°) to the main displacement direction were also observed. Locally, the P-oriented foliation can be kinked by shear bands of the normal (i.e. extensional) kink type in the same movement direction as the R_1-shears. Fractured pre-existing quartz veins and clasts are commonly oriented in the P-direction, associated to P-oriented foliation planes and shears. Continued comminution of the clasts and vein material resulted in the formation of mineral trails (Fig. 4). These form as clasts are progressively brecciated and fragments transported in the shear direction along the P-foliation to lower stress zones (Fig. 4). The better developed shear type in the CFS are Y-oriented shears, which are usually steeply dipping and parallel to the main fault boundaries (Fig. 5a). Y-shears are particularly significant because they bound the different gouge bands or lenses, and appear to have functioned as the principal movement planes. In outcrop Y-shears are widespread inside the gouge zone and commonly accompanied by localized cataclastic bands of centimetric width (Fig. 5a). R_1-shears are also present in the fault rock, but overall are less abundant than P-oriented structures (Fig. 5b). The R_1-shears are usually inclined 8–30° to the slip direction.

It is not uncommon to find carbonate (calcite and minor siderite) and/or gypsum veins in the gouge matrix or in competent rock clasts incorporated in the shear

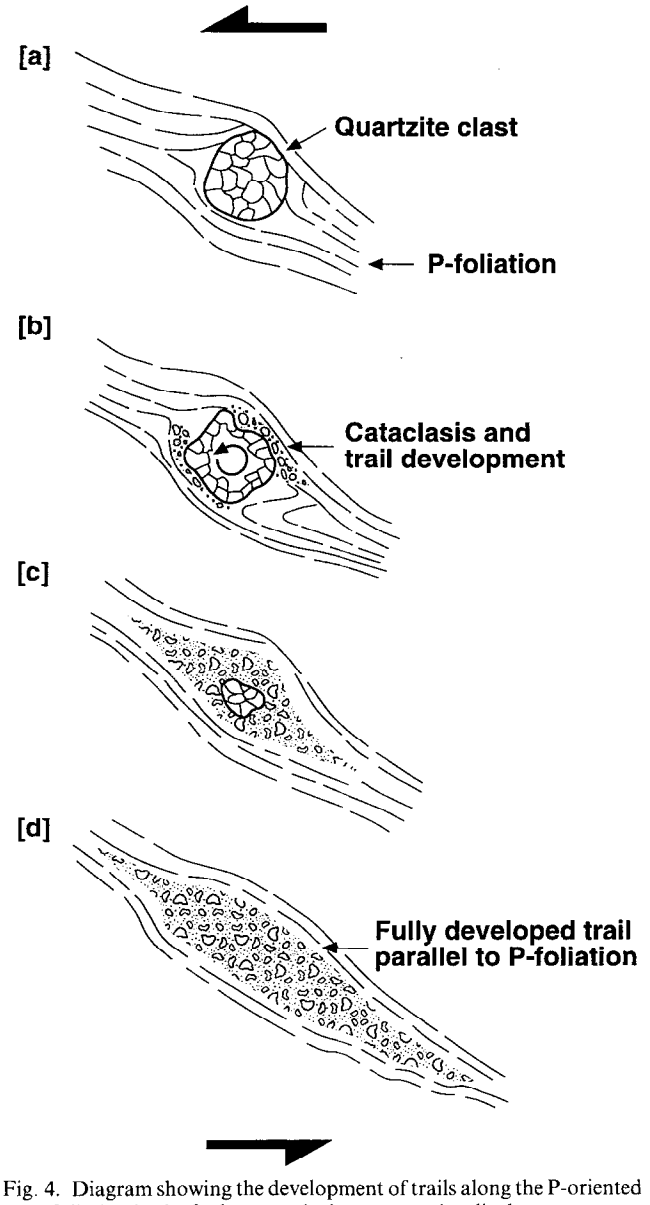

Fig. 4. Diagram showing the development of trails along the P-oriented foliation in the fault gouge during progressive displacement.

zone. The veins and fractures in the gouge matrix are usually perpendicular to the P-foliation and, therefore, attributed to tensional failure. Successive episodes of fluid activity during fault movement are recognized by cross-cutting or multiple generation individual veins, as well as by recemented microcataclasites within the fault zone.

Microstructures

The gouges developed in the Colorados fault zone exhibit a clay-rich matrix composed of fine-grained phyllosilicates such as green and blue chlorite, muscovite, montmorillonite, illite and minor kaolinite. Small angular to rounded clasts and polycrystalline fragments occur within the matrix, especially of quartz, red sandstone or quartzite, dolomite, graphitic phyllite/schist, oolitic limestone and biotite. In thin section the phyllosilicates in the matrix were observed to be preferentially oriented in the P-orientation forming a thinly spaced and penetrative foliation (Fig. 5c). Frequently, small clasts (0.1–0.5 mm) show alignment with the phyllosilicates in the matrix. P-shears developed along, or at very near angles to, the P-foliation, whereas Y-shears are observed to form mm-scale discontinuous slip planes that transect and/or deflect the P-foliation (Fig. 5c). Mineral trails and phyllosilicates can be locally re-oriented by the Y-shears (Fig. 5c), especially close to the main slip zones between the different gouge bands. Local deflections in the gouge's foliation are also related to R_1-shears (Fig. 5c), or less frequently by sets of either normal or reverse kink-bands.

Deformation in the gouges occurred mainly due to frictional sliding, kinking and diffusive mass transfer, whereas, in the microcataclasites, deformation mechanisms like grain-size reduction by brittle fracturing (intragranular and intergranular cracking) and associated grain-boundary sliding predominated. Near the main slip zones the gouge minerals, and clasts, show abundant evidence of grain-size reduction by cataclasis (mainly cataclastic flow represented by grain fracturing and frictional sliding of grain fragments). Isolated clasts can exhibit intragranular fracturing, as well as fragment rotation, and in some cases faint signs of crystal plasticity such as undulose extinction. The predominance of cataclasis over solution-transfer mechanisms appears to indicate strain rates in the Colorados shear zone were too great to be accommodated by mass transfer.

TRIAXIAL AND DIRECT SHEAR FRICTION-SLIDING EXPERIMENTS

Experimental configuration and methodology

In order to investigate the textural evolution of fault gouge structures, and their geometry, with increasing shear strains frictional-sliding experiments were carried out. The resulting microstructures and their textural evolution were then compared to those described from the field studies. Two types of rigs were used in simple shear experiments, a triaxial fluid-confining medium machine and a direct shear unconfined apparatus for larger strain experiments. The experiments were carried out by placing natural and 'synthetic' fault gouge between two intact rock blocks and shearing it under various combinations of confining pressures (50–300 MPa) and shear strains. Tests were run under a strain rate of 10^{-5} and $10^{-1}\,s^{-1}$ in the triaxial rig, whereas in the direct shear tests experiments shear strains of up to 14 were recorded under normal stresses of 25–50 MPa. In the majority of the experiments, a 0.5 mm layer of fault gouge paste was placed on a 30° or 45° sawcut surface made in an intact rock cylinder or plate. Triaxial experiments used serpentinite for the cylinders,

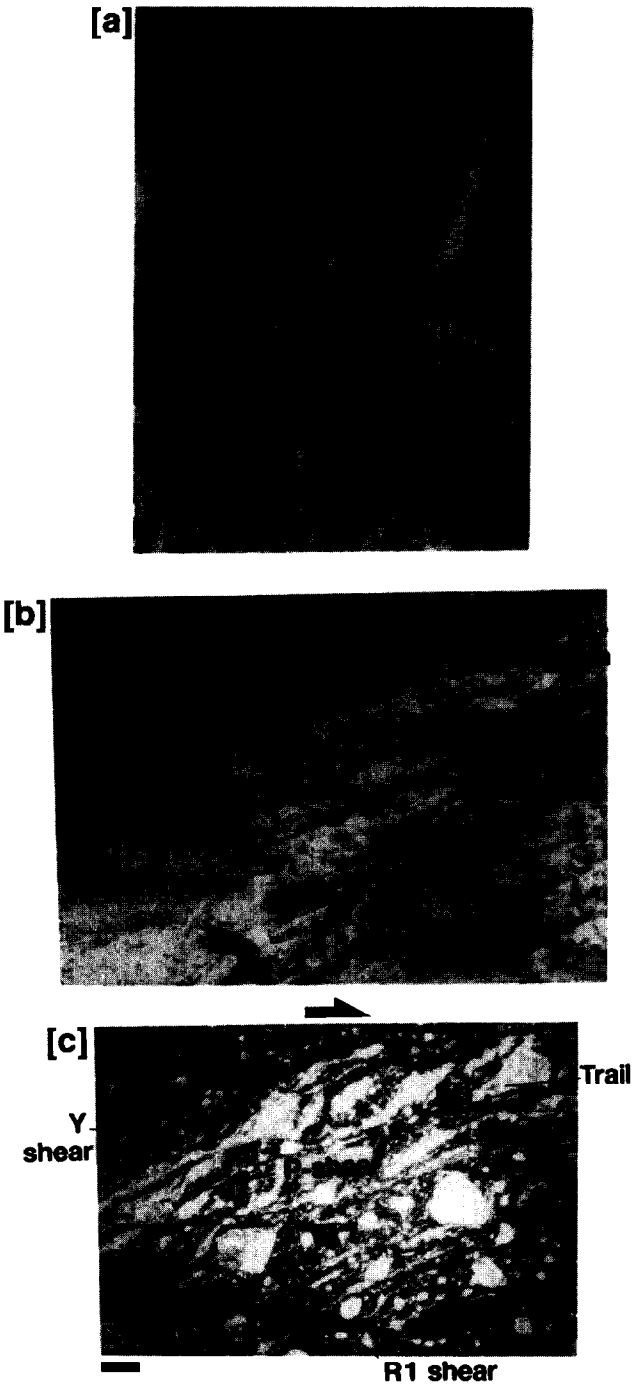

Fig. 5. Photographs of fault gouges in the Colorados fault. (a) Field photograph. Clay-rich phyllite gouge with deformed sandstone and marl–phyllite clasts. Note the pervasive Y-shears and the millimetric–centimetric colour bands oriented parallel the Y-shears. Vertical section; hammer is approximately 35 cm long. (b) Field photograph. Clay-rich black to purple schist and sandstone gouge exhibiting deformed sandstone clasts stretched and boudinaged along P-shears. Note the pervasive P-foliation within the schist gouge and the formation of mineral trails oriented parallel the P-shears. Two late R_1-shears are seen transecting the P-foliation and P-shears (including the elongate clasts and mineral trails) to the right of the hammer. Horizontal section; hammer head is approximately 12 cm long. (c) Photomicrograph (Alhama de Murcia fault). Clay-rich fault gouge showing well-developed P-foliation, as well as P- and Y-shears. Note how the mineral trails are oriented along the P-orientation and are deflected by the cross-cutting Y-shears. An R_1-shear occurs at the lower part of the photograph oriented at a low angle to the border. Scale is 1 mm long.

whilst in the direct shear rig black gabbro was used for the plates. Experiments run in the triaxal fluid-confining medium rig were terminated after a pre-determined displacement had occurred (2 mm). This was due to the experimental set-up that required the specimen to be encased in a copper jacket which tends to rupture as a result of the specimen failure.

The 'synthetic' gouge was prepared from a mixture of kaolinite and silt-grade quartz in various proportions (10, 50 and 90%). The gouge was then prepared by mixing water to the clay–quartz mixture until it formed a stiff paste. This gouge paste was then placed between the rock plates and dried at around 90°C before testing. Natural gouge samples were ultrasonically disaggregated before being deformed, and had the coarser fraction (>0.2 mm) removed. The finer fraction was dampened to form a paste as with the 'synthetic' gouges. Natural gouges tested in the triaxial rig experiments include the chlorite-rich Colorados fault gouge (Fig. 2) and the kaolinite-rich Alhama de Murcia fault gouge (Fig. 3). Chlorite-rich Colorados fault gouge, red sandstone Colorados fault gouge, kaolinite-rich Alhama de Murcia fault gouge, as well as a montmorillonite-rich fault gouge from the San Andreas fault, California, were tested in the direct shear rig. After the experiments, the deformed gouge was sectioned parallel to the long axis of the sample and prepared into thin sections for petrographic analysis.

Textural observations

A four-stage textural development was observed during the friction-sliding experiments. To observe the development of the microstructures, several experiments using the same boundary conditions were carried out and stopped after various amounts of strain. No major differences were seen in the deformation fabric developed in different experiments at comparable strain levels but at different confining pressures. Similar results were obtained for tests on natural and synthetic gouges (Fig. 6). A summary of the four-stage gouge textural development with increasing strain is presented in Fig. 7.

During early *stage I* unsheared samples have a poorly defined phyllosilicate alignment parallel to the sawcut surface (i.e. the Y-orientation), with rare poorly developed normal kinks which formed at high angles to the gouge–intact rock interface. This sawcut-parallel fabric corresponds to a flattening fabric formed during the preparation and assembly of the specimen inside the rig prior to the beginning of the experiment (Fig. 7a). From the beginning of the experiment, even at low strains, phyllosilicates within the matrix start to rotate in the opposite sense to the shear direction away from the maximum incremental elongation direction ($<5°$ from the Y-direction). This resulted in the formation of a P-oriented foliation.

Further phyllosilicate rotation into the P-orientation

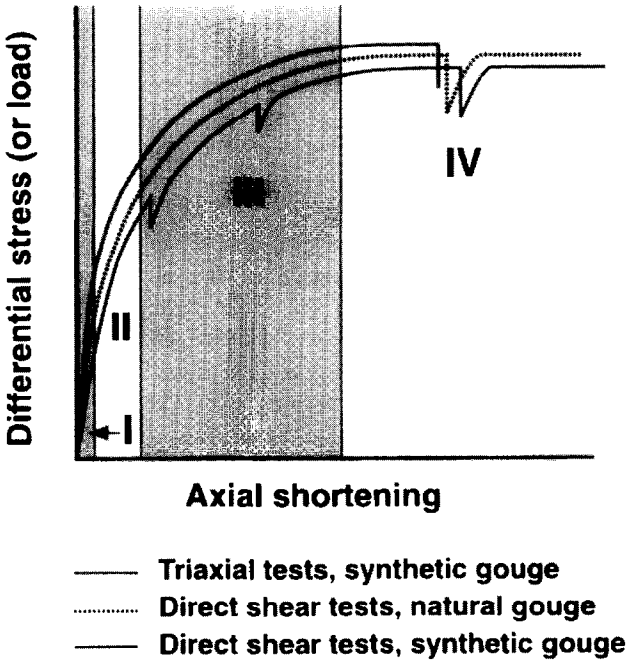

Fig. 6. General stress (or load)–shortening plots indicating the stages of textural development in the gouges during laboratory frictional tests.

occurs during early *stage II*, producing an increasingly pronounced planar fabric at angles that varied from 5° to approximately 15° to the sawcut surface (Figs 7b & 8a). R_1-shears also started to develop. The P-oriented foliation appeared not to be affected by further increases in shear strain, but by localized inter-crystallite sliding. This resulted in the formation of P-shears that with increasing strain propagated along the foliation (Fig. 8a). Often R_1-shear nucleation was localized by grains or other heterogeneities in the gouge matrix, whereas P-shears re-utilized the existing P-foliation. As shear strain increased rare reverse and normal kink-bands developed at high angles to the shear direction, usually associated with localized perturbations in the matrix such as quartz grains (Fig. 8a). Normal kinks developed at angles between 10° and 20° to the sliding direction, exhibiting the same sense of movement as R_1-shears.

Stage III was characterized by the full development of the R_1-shears and, to a lesser extent, the P-shears, as well as the reverse and normal kink-bands (Fig. 8b). Reverse kink-bands developed in two main orientations, either $<45°$ or $>45°$ to the shear direction. Kink-bands that were first nucleated near quartz grains subsequently propagated through the phyllosilicate-rich matrix (Fig. 8b), sometimes kinking pre-existing R_1- and P-shears (Fig. 7c). This blocked further displacements along the kinked shear plane. In other instances it was the development of sub-parallel shears that limited the area of kink-band growth (Fig. 8b), with kink-bands being limited in their final length or exhibiting different orientations across a shear plane. Occasionally, the R_1-shears were also observed to curve towards the sawcut–gouge boundary when reaching it (Fig. 7c). Typically, the angle between the R_1-shears and the sawcut boundary was not constant, but showed variations ($\pm 5°$) even within the same tested gouge specimen.

Sudden localized failure or instability initiation, which led to complete gouge failure accompanied by stress drops, occurred during *stage IV* (Fig. 6). At this stage textural development reached its final configuration (Figs 7d & 8c). Slip instabilities developed along the sawcut–gouge boundary or as cross-gouge structures (Fig. 8c), which invariably led to cross-gouge failure (i.e. specimen failure by movement being transferred across the gouge). This type of fabric represents an end-member where deformation is concentrated along a narrow zone, resulting in extreme shear localization and stick–slip gouge behaviour. Sudden failure was only achieved in two of the triaxial tests, but occurred in most direct shear tests. In one experiment cross-gouge failure was achieved by means of a complex set of linked R_1-shears (Fig. 8c), whereas in the other by a P-shear. Y-shears were not observed to develop in any of the experiments. Continued shear after cross-gouge failure was only possible in the direct shear tests as in the triaxial rig specimen failure resulted in the rupture of the encasing jacket.

To investigate the effect of lithological banding in the development and geometry of gouge structures, experiments were carried out in which a layer of synthetic gouge (90% kaolinite and 10% quartz) was placed along a layer of natural fault gouge (either from the Colorados fault or the Alhama de Murcia fault). Deformation conditions were the same as in previous direct shear tests, with the layered gouge experiments also showing a four-stage textural development and similar deformation fabric and microstructures. Similar textures formed in the two different gouges, as if the gouges had been deformed separately. This indicates that different gouge zones in natural fault zones behave as independent units, with their response to deformation depending on the nature and properties of the rock type. Unlike the previous experiments, however, R_1-shears were sometimes observed to bend asymptotically towards the 'lithological banding' in the centre of the specimen developing a more sigmoidal geometry.

PHYSICAL CLAY MODELLING

Experimental configuration and methodology

To better understand the evolution of secondary shear fracture patterns, especially P-oriented shears, in transpressional strike-slip systems three-dimensional clay-box modelling of localized transpressional deformation was carried out. Other aims of the clay-box modelling were to investigate the progressive development and determine a sequence of secondary shear formation in transpressional shear zones. The experimental apparatus consisted of a clay-box with two movable basal plates, connected via worm screws to two motors generating a left-lateral

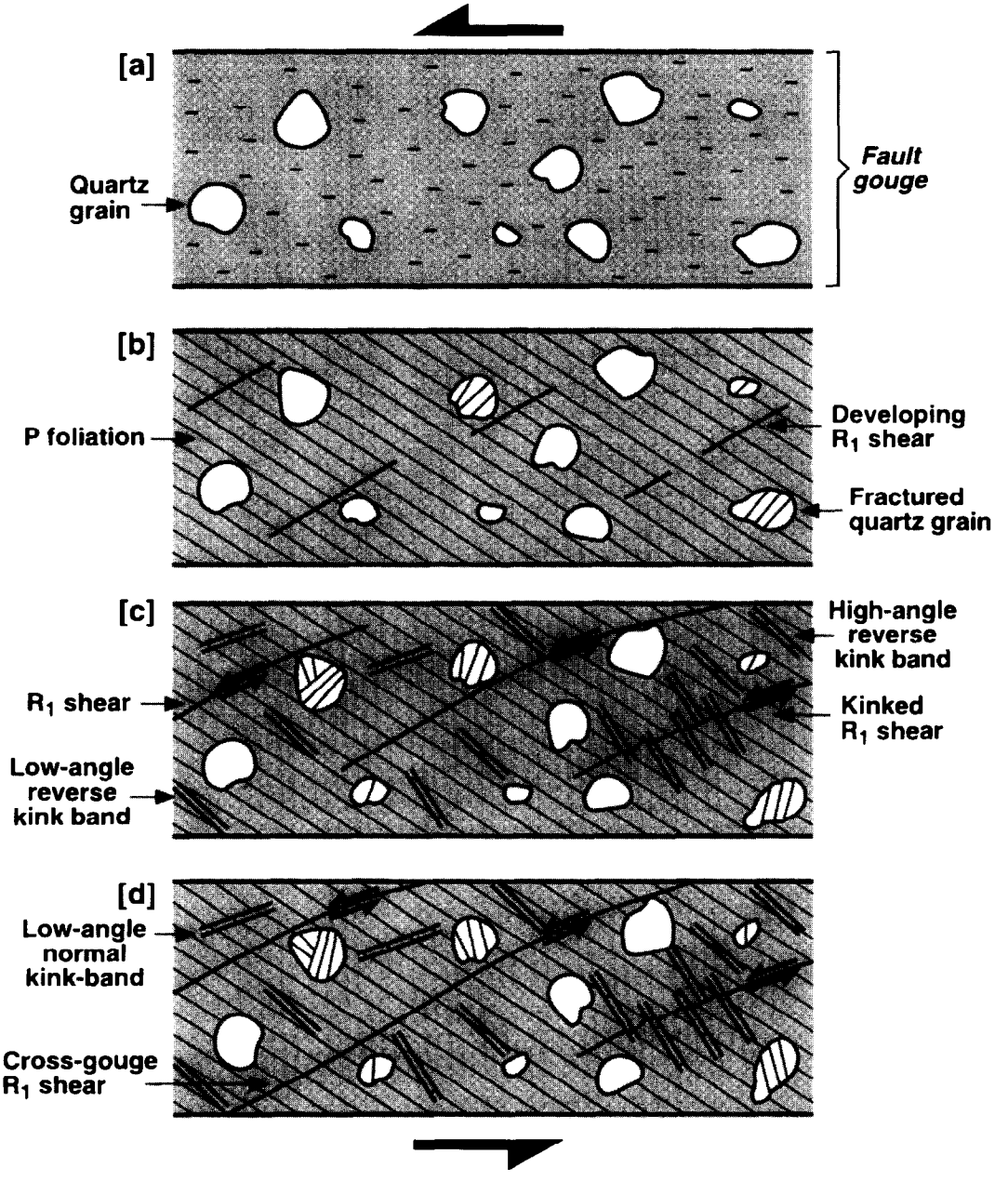

Fig. 7. Schematic diagram illustrating the textural evolution in synthetic gouges with increasing strain. (a) During stage I a poorly developed sawcut parallel anisotropy is formed. (b) In stage II the anisotropy rotates and intensifies forming a P-foliation. R_1-shears start to form and some of the grains show evidence of internal fracturing. (c) R_1-shears propagate and kink-band formation fully starts at stage III. Fracturing of grains increase, as well as grain rotation. (d) Stage IV is marked by instability initiation, at first along the sawcut–gouge boundary and then by cross-gouge failure along R_1-shears. No Y-shears developed during the experiments.

displacement (Fig. 9). The geometry of the movable basal plates mimicked a restraining bend producing localized transpressive strains during fault motion (Fig. 9a & b). The lateral offset between the two plates was of 10 cm. Base plates with different step-over angles were used (30°, 45°, 60° and 90°), with each experimental set-up being repeated at least twice with reproducible results. The rate of movement of the motors was 4.16×10^{-3} cm s^{-1}. The clay-box dimensions were $85 \times 40 \times 10$ cm at the beginning of the experiments with all models being run to a maximum displacement of 15 cm.

Dry white china clay was used in the models, mixed at a proportion of 1.5 parts of clay to 1 part of cold water. The clay consists mainly of kaolinite, and minor quartz, with a grain size <60 μm. In the experiments a 10 cm thick tabular sheet of clay was laid inside the clay-box, directly onto the basal plates. A passive grid was placed on the top surface of the clay cake using graphite powder forming a 2 cm square pattern. A 35 mm camera placed above the model recorded the progressive deformation on the surface of the clay model through sequential time-lapse photography. Further analysis was then performed

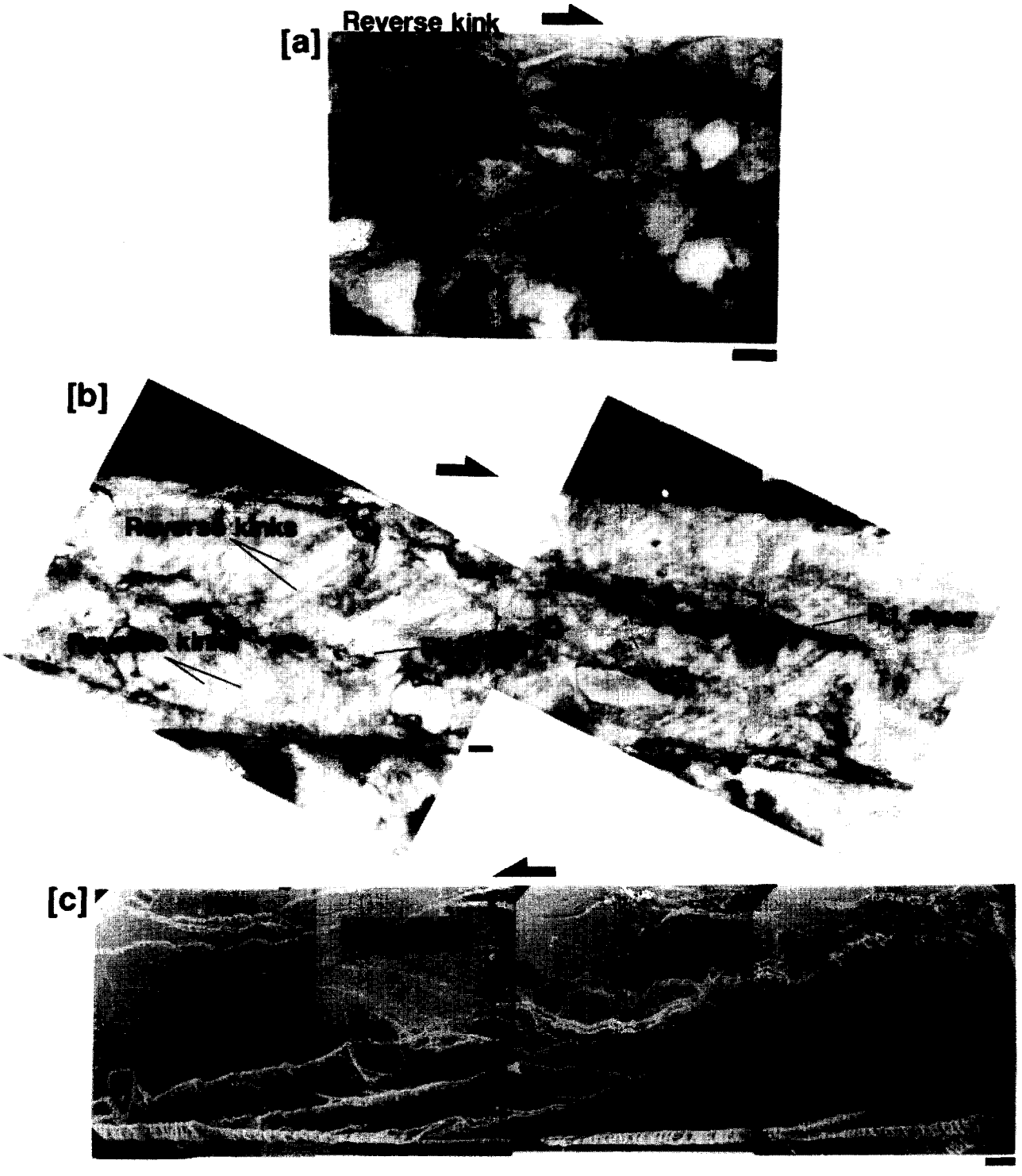

Fig. 8. Photomicrographs of experimentally deformed synthetic clay-rich gouges. (a) Optical photomicrograph. Clay (kaolinite) gouge matrix showing the development of normal and reverse kink-bands and irregular shear planes that appear to have a P-orientation. Scale is 0.1 mm long. (b) Optical photomicrograph. Well-developed R_1-shears and reverse kink-bands at stage III of textural development. Note the different kink orientations on either side of the R_1-shear on the lower-left and the offset kinks at the tip of the R_1-shear on the right. Scale is 0.1 mm long. (c) Scanning electron micrograph mosaic of a polished section of deformed synthetic gouge after etching with an argon ion beam. Deformed fault gouge exhibiting the development of a complex array of throughgoing R_1-shears and subsidiary P-shears connecing the former (some R_1-shears curve towards a P-orientation; see centre of the mosaic). The internal texture is also characterized by pervasive, but less significant, P- and R_1-shears. High relief clasts are quartz grains. Quartz fracturing is common, as well as high-angle normal and reverse kink-bands (note that the kink-bands are usually associated with quartz grains). Scale is 0.1 mm in length.

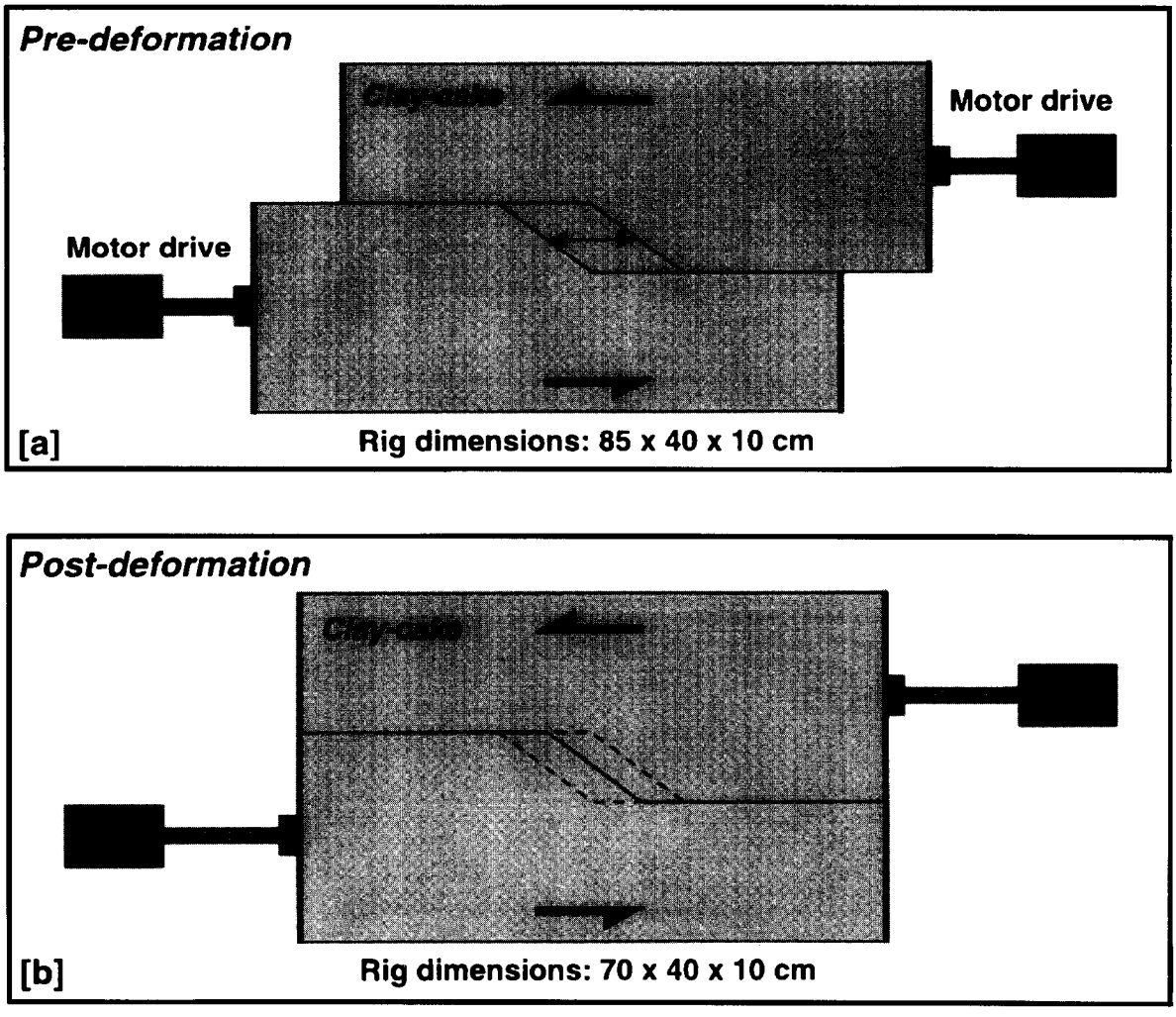

Fig. 9. Schematic diagram of the deformation rig. (a) Pre-deformation configuration. (b) Post-deformation configuration.

using the photographs. A total of 12 experiments were carried out using base plates with different geometries.

Model results

The models consistently produced a push-up zone with the geometry of a symmetric dome in cross-section and a fracture pattern consistent with the fault geometries observed in the CFS. P-oriented shear fractures formed in the zone of transpression above the offset zone, whereas along the straight portion of the boundary faults R_1-Riedel shears developed. The geometry of the push-up dome is strongly dependent on the base plate shape, especially at the initial increments of displacement. A summary of the transpressional clay-modelling results showing the main stages of deformation and structures developed in the experiments is presented in Fig. 10.

Initial deformation produced a linear set of en échelon R_1-oriented shears in the clay above the straight sections of the base plates, and a push-up dome structure above the base plates offset (the zone of transpression; Fig. 10a). As displacement increased, P-shears developed in the push-up zone and progressively coalesced with the en échelon R_1-shears along the linear shear zones that bordered the transpressional central region (Figs 11b & 12b). These shear zones propagated further along-strike and overlapped at the centre of the clay-cake defining the full length of the push-up dome. At 5 cm of displacement Y-oriented shears also started to nucleate in the uplifted zone (Figs 11b & 12b). Y- or P-shears developed depending on the offset angle of the basal plates being used. Typically, Y-shears were formed in the experiments using plates with step-over angles $<30°$.

Further increments of displacement caused the shears to propagate along-strike towards the P-orientation (Fig. 10b). Propagation causes some of the shears to locally acquire a sigmoidal shape, but most shears remain relatively straight (Figs 11c & 12c). As a result, a well-developed system of overlapping P-shears is formed that extends across the push-up zone towards the bordering shear zones (Figs 11c & 12c). With increasing shearing (8 cm displacement) a few Y- and, especially, R_1-shears (cross-shears) started to propagate in the transpressional

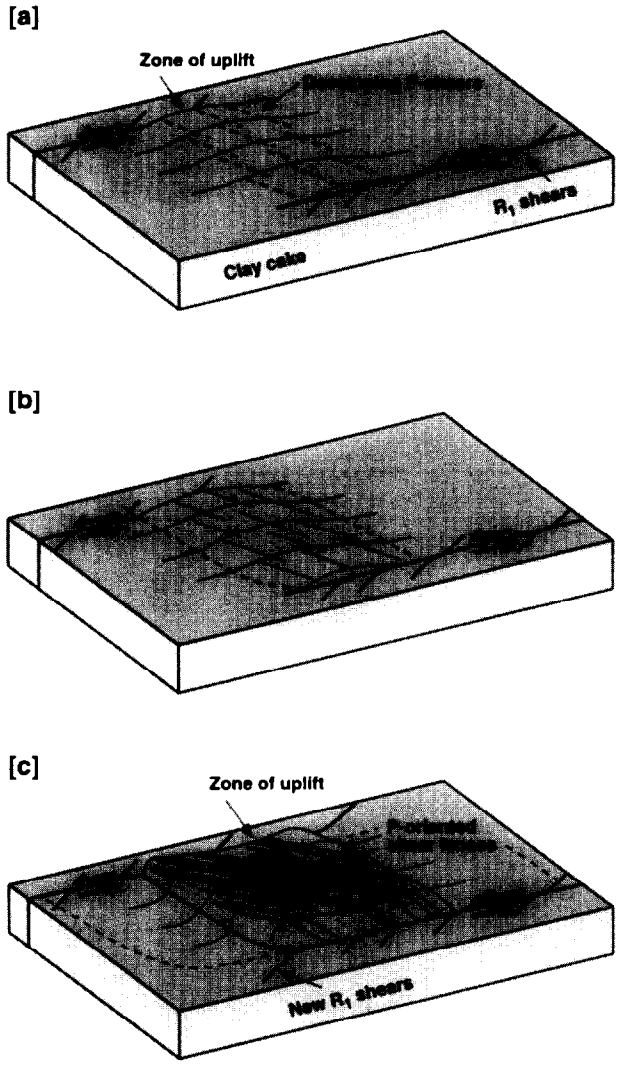

Fig. 10. Evolution diagram showing the development of secondary shear structures and shear lenses during transpressional clay modelling experiments. See text for a full description.

area. These shears then linked to the existing P-shears producing elongated shear lenses parallel to the P-direction that could extend across the uplifted zone. Less numerous, relatively small shear lenses occurred along the border shear zones. At 11 cm of displacement new P-shears started to propagate from near the tip of the bordering shear zones to the opposing shear zone (Fig. 10b). New R_1-shears also started to form at the tip zones of the border faults. In the last two increments (14–15 cm) a throughgoing P-oriented shear developed across the uplifted zone linking the border shear zones (Figs 11d & 12d). At the same time the R_1-shears at the tip zones of the border faults started grow laterally causing the shear zones to curve towards the R_1-direction (Figs 12d & 13d).

Often the P-shears in the uplifted area displayed a component of reverse displacement that increased with increasing bulk shear, although some shears exhibited a normal displacement component. The P-shears close to the limits of the transpressional zone, however, invariably exhibited a component of reverse displacement. The P-shears varied in length between <2 and 25 cm, and displayed along-strike displacements of the order of up to 1.5–2.0 cm. During the experiments the push-up zone was observed to extend parallel to the direction of movement and increase in height with increasing transpressional strain (see Figs 11 & 12). Therefore, the final length and height of the push-up dome depends on the amount of movement and the offset angle of the base plate. The shortest was associated with a 90° step-over angle and the longest with a 30° step-over angle (maximum dome length produced with the experimental configuration used was approximately 45 cm).

Previous analogue modelling studies of transpressional zones include Richard and Cobbold (1990) and Richard *et al.* (1995). The experiments used sand as the main modelling material in contrast to clay in our models which allows for the development of sharper faults and greatly increases the limit of visual resolution. In both sets of former experiments secondary P-oriented shear fractures have developed associated with more prominent Y-oriented faults (see Richard and Cobbold, 1990, fig. 8a & c; Richard *et al.*, 1995, fig. 18b). However, in Richard *et al.* (1995) deformation was continued until the pop-up formed above the zone of transpression became detached from the base plate and rotated about a vertical axis. This caused the generation of antithetic Riedel-shears within the pop-up region that overprinted the previously existing Y- and P-shears (see Richard *et al.*, 1995, fig. 18c).

DISCUSSION

Comparison of transpressional geometries from the field and from laboratory experiments

On a regional scale the CFS exhibits an internal architecture formed by a linked system in which displacement is partitioned between *Y*-oriented strike-slip and *P*-oriented reverse-slip fault zones. The regional strike of the foliation, fold axis trends in the field, as well as the strike direction of the second-order faults, are all consistent in orientation with a transpressional setting for the CFS. Previous reports of transpressional systems in the literature have also described a widespread occurrence of P-oriented shears (Swanson, 1988; Moore and Byerlee, 1991; Cunningham *et al.*, 1996), as well as intrusions of P-oriented granitic bodies in between regional-scale P-shears (Tikoff and Teysser, 1992; Cunningham, 1995). Second-order fault patterns made up by P-shears and subordinate R_1-shears, as well as shear lenses that tended to be aligned towards the P-shear direction, were produced in our clay-box analogue models of transpression. The fact that the geometry of subsidiary shear fractures in nature and in the experiments are so remarkably similar suggests a common mechanical behaviour for transpressional faults over four

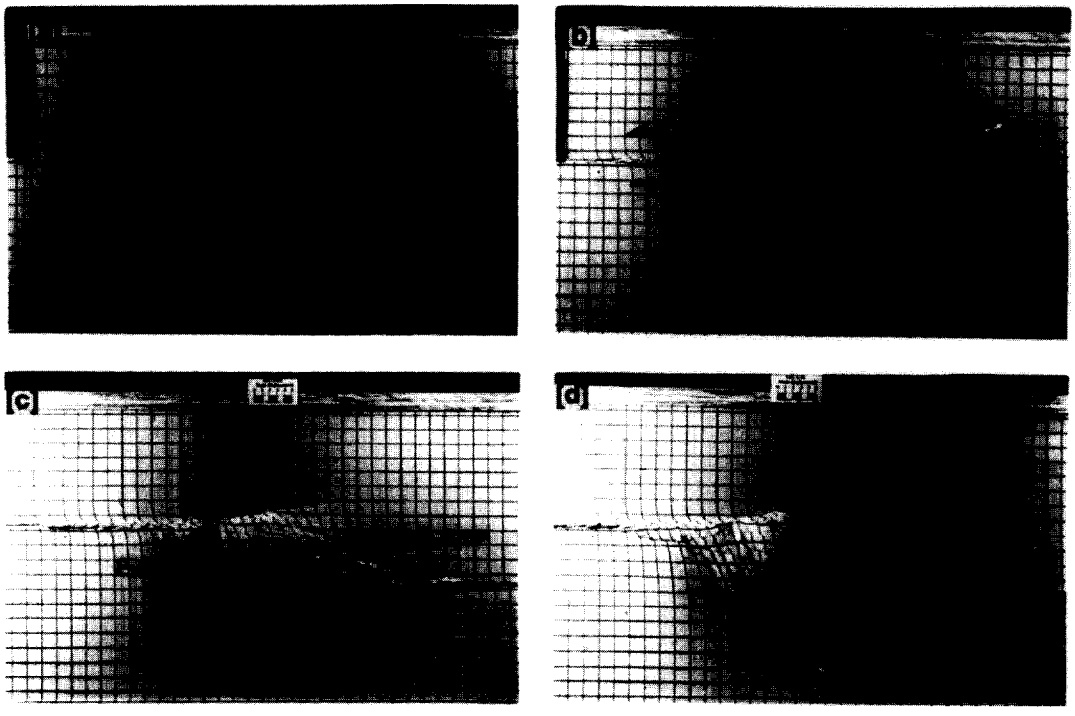

Fig. 11. Sequential photographs showing the progressive evolution of a transpressional clay experiment with a 30° step-over angle (TPC-6). (a) Underformed state. (b) 5 cm displacement. (c) 11 cm displacement. (d) 15 cm displacement. See text for a full description.

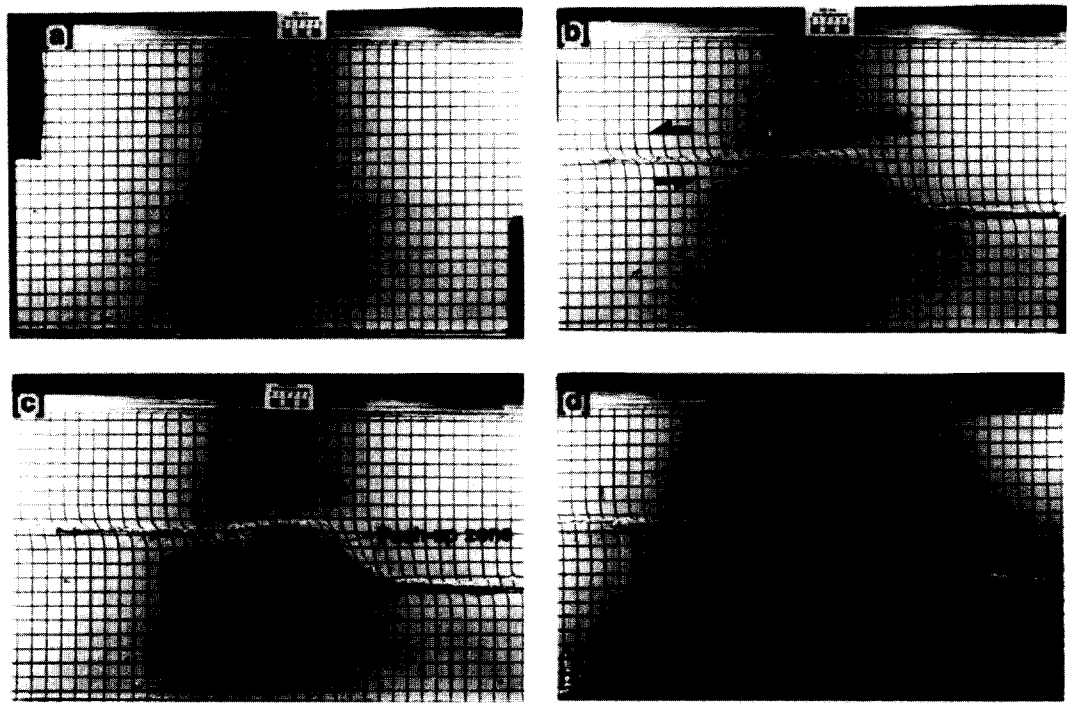

Fig. 12. Sequential photographs showing the progressive evolution of a transpressional clay experiment with a 45° step-over angle (TPC-8). (a) Undeformed state. (b) 5 cm displacement. (c) 10 cm displacement. (d) 15 cm displacement. See text for a full description.

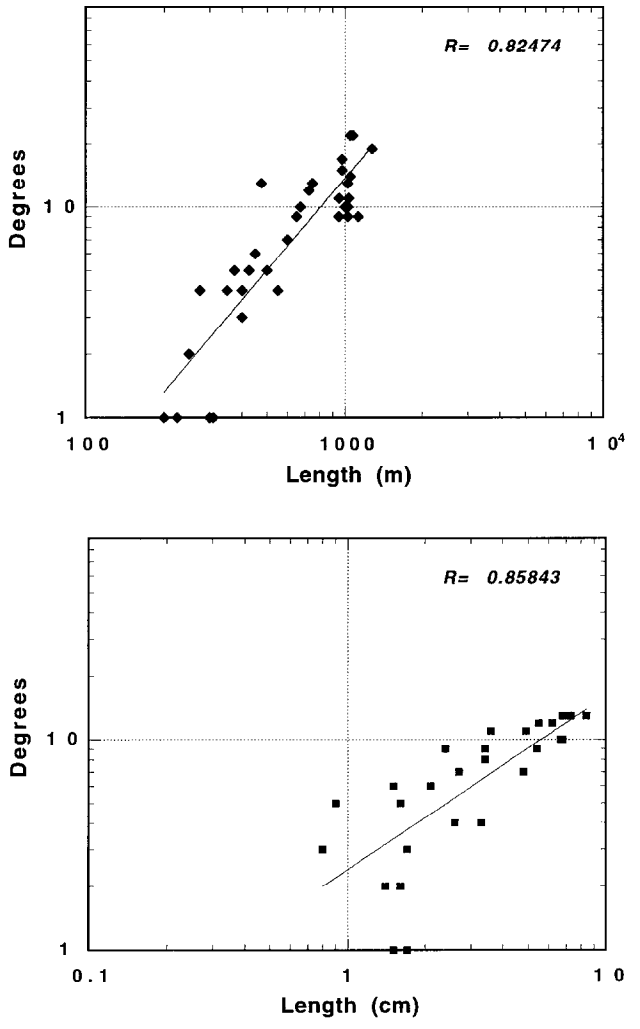

Fig. 13. Orientation–size log–log plots for shear lenses mapped within the CFS and developed in the clay experiments. (a) CFS case. (b) Clay models.

orders of magnitude. Moreover, our experimental results, in addition to the CFS case study and other examples from the literature, are in good agreement with the hypothesis that P-shears are preferentially developed during transpressional deformation and are a diagnostic feature of this deformation regime.

The orientation of the shear lenses (defined as the angle between the lens' longest axis and the mean displacement direction) plotted against the length of their longest axis for shear lenses in the CFS and in the analogue models is presented in Fig. 13. Lenses located close to the border faults or major first-order faults were not included in the plots as their orientation is controlled by their proximity to the main faults. Both plots exhibit a linear power-law (logarithmic) scaling relationship, well constrained by correlation coefficients of 0.83 and 0.85 (Fig. 13a & b). Differences in the correlation factors and slopes between the plots may be a result of different degrees of freedom for rotation, or alternatively of different mechanisms of fault propagation and lens formation, in the experiments and in nature. Nevertheless, the scaling relationships suggest that the direction of individual shear lenses is size-dependent, even though shear lenses usually develop parallel to the P-oriented faults that dominate the architecture of the fault zone. This also means that the resulting internal architecture of the fault zone is directly influenced by the size (length) of the shear lenses formed within it. Moreover, the range of values for shear lens orientation in the CFS and in the clay-box experiments suggest that differential block rotation occurred during deformation. Smaller lenses appear to have rotated more than longer ones as their orientation is closer to the displacement direction (Fig. 13a & b), indicating that shear lens size influences the amount of rotation that each individual lens can undergo inside the fault zone.

CONCLUSIONS

A characteristic shear fracture pattern was observed in the CFS at various scales, from regional to microscopic, typically showing first-order Y-oriented faults, a P-oriented foliation and a widespread occurrence of P-oriented second-order faults in contrast to R_1-shears. Clay-box analogue modelling of transpressional fault zones also exhibited faults with P-orientation that predated or were synchronous to the development of R_1-shears. Shear lenses also tended to be aligned towards the P-shear direction. In the models, P-shears formed within the push-up zone in the centre of the model and grew during successive deformation increments. The P-oriented shear lenses developed mainly through the linkage of non-coplanar P-shears. P-shears invariably terminated against the two main boundary shear zones and are younger than the first-order boundary faults. In the case of the CFS, fault-zone geometry was probably also controlled at first by the development of the first-order faults, and was followed by the formation of the P-oriented second-order internal faults as documented in the analogue models. Localized block rotation of P-oriented lenses was observed in the experiments together with the propagation of the secondary faults along strike. Internal rotation of the shear lenses about a vertical axis is also interpreted to have occurred in the CFS as suggested by the sigmoidal geometry of some of the second-order P-shears. In addition, the clay-box modelling results indicate that complex transpressional fault zones such as the CFS develop through multiple faulting events, along-strike propagation of faults of different orders and fault-block rotation.

Results from the frictional experiments show an early orientation of phyllosilicates in the gouge matrix towards the P-direction, generating a P-foliation. Further deformation can cause the foliation anisotropy to accommodate slip, and thus become a P-shear. These results also suggest that P-shears must be common features, and even predominate over R_1-shears, in transpressional shear zones. This is consistent with the proposition that P-shears are preferentially developed during transpres-

sional/oblique-convergent deformation, and can be used in the identification of transpressional fault zones in the field. From the observed development and orientation of the P-oriented foliation, and the associated P-shears, in the frictional experiments it is clear that they tend to develop close to the main flattening direction. The frictional experiments were conducted under general simple shear and, therefore, we expect reactivation of P-foliation planes into P-shears to be even more prevalent under transpression.

Acknowledgements—J. V. A. Keller would like to thank J. R. Henderson for helpful comments on a previous version of this manuscript and stimulating discussions on transpression. S. H. Hall is grateful to E. Rutter for ideas and useful discussions during his work on the faults of southern Spain. The paper has also benefited considerably from thoughtful reviews and comments by Michael Naylor and James Evans and Associate Editor Richard Lisle. The authors would also like to thank B. Adams for technical support and D. Mellor for assistance during laboratory work at Royal Holloway. Supported by the Fault Dynamics Project, which is sponsored by ARCO British Limited, PETROBRAS U.K. Ltd, BP Exploration, Conoco (U.K.) Limited, Mobil North Sea Limited and Sun Oil Britain. Fault Dynamics publication 70.

REFERENCES

Bakker, H. E., de Jong, K., Helmers, H. and Biermann, C. (1989) The geodynamic evolution of the internal zone of the Betic Cordilleras (southeast Spain): a model based on structural analysis and geothermobarometry. *Journal of Metamorphic Geology* **7**, 359–381.

Banks, C. J. and Warburton, J. (1991) Mid-crustal detachment in the Betic system of southeast Spain. *Tectonophysics* **191**, 275–289.

Bartlett, W. L., Friedman, M. and Logan, J. M. (1981) Experimental folding and fracturing of rocks under confining pressure. Part IX. Wrench faults in limestone layers. *Tectonophysics* **79**, 255–277.

Chester, F. M., Evans, J. P. and Biegel, R. L. (1993) Internal structure and weakening mechanisms of the San Andreas Fault. *Journal of Geophysical Research* **98**, 771–786.

Cunningham, W. D. (1995) Orogenesis at the southern tip of the Americas: the structural evolution of the Cordillera Darwin metamorphic complex, southernmost Chile. *Tectonophysics* **244**, 197–229.

Cunningham, W. D., Windley, B. F., Dorjnamjaa, D., Badamgarov, J. and Saandar, M. (1996) Late Cenozoic transpression in southwestern Mongolia and the Gobi Altai–Tien Shan connection. *Earth and Planetary Science Letters* **140**, 67–81.

Doblas, M. and Oyarzun, R. (1989) Neogene extensional collapse in the Western Mediterranean (Betic–Rif Alpine orogenic belt): Implications for the genesis of the Gibraltar arc and magmatic activity. *Geology* **17**, 430–433.

Evans, J. P. (1988) Deformation mechanisms in granitic rocks at shallow crustal levels. *Journal of Structural Geology* **10**, 437–443.

Evans, J. P. (1990) Textures, deformation mechanisms, and the role of fluids in the cataclastic deformation of granitic rocks. In *Deformation Mechanisms, Rheology and Tectonics*, eds R. J. Knipe and E. H. Rutter, pp. 29–39. Geological Society Special Publication **54**.

Fournier, M. (1980) Le bassin de Níjar-Carboneras (Cordillères bétiques). Néotectonique: Étude des Diaclases. Unpublished Ph.D. thesis, Université de Paris VII.

Freund, R. (1974) Kinematics of transform and transcurrent faults. *Tectonophysics* **21**, 93–134.

García-Hernández, M., Lopez-Garrido, A. C., Rivas, P., Sanz de Galdeano, C. and Vera, J. A. (1980) Mesozoic palaeogeographic evolution of the external zones of the Betic Cordilleras. *Geologie en Mijnbouw* **59**, 155–168.

Hall, S. H. (1983) Post Alpine tectonic evolution of S.E. Spain and the structure of fault gouges. Unpublished Ph.D. thesis, Imperial College, University of London.

Hempton, M. R. and Neher, K. (1986) Experimental fracture, strain and subsidence patterns over en echelon strike-slip faults: implications for the structural evolution of pull-apart basins. *Journal of Structural Geology* **8**, 597–605.

Keller, J. V. A., Hall, S. H., Dart, C. J. and McClay, K. R. (1995) The geometry and evolution of a transpressional strike-slip system: the Carboneras fault, SE Spain. *Journal of the Geological Society of London* **152**, 339–351.

de Larouzière, F. D., Bolze, J., Bordet, P., Hernández, J., Montenat, C. and Ott D'estevou, P. (1988) The Betic segment of the lithospheric Trans-Alboran shear zone during the late Miocene. *Tectonophysics* **152**, 41–52.

Logan, J. M., Friedman, M., Higgs, N. G., Dengo, C. and Shimamoto, T. (1979) Experimental studies of simulated gouge and their application to studies of natural fault zones. *U.S. Geological Survey Open-file Report* **79-1239**, 305–343.

Lonergan, L. (1993) Timing and kinematics of deformation in the Malaguide Complex, Internal Zone of the Betic Cordillera. *Tectonics* **12**, 460–476.

Mandl, G., de Jong, L. N. J. and Maltha, A. (1977) Shear zones in granular material. *Rock Mechanics* **9**, 95–144.

Montenat, C., Ott D'estevou, P. and Masse, P. (1987) Tectonic–sedimentary character of the Betic Neogene basins evolving in a crustal transcurrent shear zone (SE Spain). *Bulletin des Centres de Récherches Explororation–Production Elf Aquitaine* **11**, 1–22.

Moore, D. E. and Byerlee, J. (1991) Comparative geometry of the San Andreas fault, California, and laboratory fault zones. *Bulletin of the Geological Society of America* **103**, 762–774.

Moore, D. E., Summers, R. and Byerlee, J. D. (1989) Sliding behaviour and deformation textures of heated illite gouge. *Journal of Structural Geology* **11**, 329–342.

Naylor, M. A., Mandl, G. and Sijpesteijn, C. H. K. (1986) Fault geometries in basement-induced wrench faulting under different initial stress states. *Journal of Structural Geology* **8**, 737–752.

Platt, J. P. and Vissers, R. L. M. (1989) Extensional collapse of thickened continental lithosphere: a working hypothesis for the Alboran Sea and the Gibraltar arc. *Geology* **17**, 540–543.

Richard, P. and Cobbold, P. (1990) Experimental insights into partitioning of fault motions in continental convergent wrench zones. *Annales Tectonicae* **4**, 35–44.

Richard, P. D., Naylor, M. A. and Koopman, A. (1995) Experimental models of strike-slip tectonics. *Petroleum Geoscience* **1**, 71–80.

Rutter, E. H., Maddock, R. H., Hall, S. H. and White, S. H. (1986) Comparative microstructures of natural and experimentally produced clay-bearing fault gouges. *Pure and Applied Geophysics* **124**, 3–30.

Sanz de Galdeano, C. (1990) Geologic evolution of the Betic Cordilleras in the western Mediterranean, Miocene to present. *Tectonophysics* **172**, 107–119.

Swanson, M.T. (1988) Pseudotachylite-bearing strike-slip duplex structures in the Fort Foster Brittle Zone, S. Maine. *Journal of Structural Geology* **10**, 813–828.

Tchalenko, J. S. (1970) Similarities between shear zones of different magnitudes. *Bulletin of the Geological Society of America* **81**, 1625–1640.

Tchalenko, J. S. and Ambraseys, N. N. (1970) Structural analysis of the Dasht-e-Bayaz (Iran) earthquake fractures. *Bulletin of the Geological Society of America* **81**, 41–60.

Tikoff, B. and Teysser, C. (1992) Crustal-scale en echelon 'P-shear' tensional bridges: A possible solution to the batholitic room problem. *Geology* **20**, 927–930.

Weijermars, R. (1991) Geology and tectonics of the Betic Zone, SE Spain. *Earth Science Reviews* **31**, 153–236.

Wilcox, R. E., Harding, T. P. and Seely, D. R. (1973) Basic wrench tectonics. *Bulletin of the American Association of Petroleum Geologists* **57**, 74–96.